ZnO AND $MoSe_xO_y$ MODIFIED TiO_2 NANOTUBES FOR PHOTOELECTROCHEMICAL AND SENSING APPLICATIONS

NG SIOW WOON

UNIVERSITI SAINS MALAYSIA

2018

ZnO AND $MoSe_xO_y$ MODIFIED TiO_2 NANOTUBES FOR PHOTOELECTROCHEMICAL AND SENSING APPLICATIONS

by

NG SIOW WOON

Thesis submitted in fulfilment of the requirements
for the degree of
Doctor of Philosphy

September 2018

ACKNOWLEDGEMENT

First and foremost, I would like to express my earnest gratitude to my supervisor Assoc. Prof. Dr. Yam Fong Kwong for his constant guidance, patience, and support. We shared many ups and downs throughout the years I spent in this group. This work would not have been completed on time without his vital contribution.

I am grateful to my co-supervisor Prof. Dr. Zainuriah Hassan, for her guidance and insightful advice, despite her busy schedule. She has inspired me in many ways, as a leading woman scientist in this country.

I am indebted to Dr. Jan M. Macak, my host-supervisor, for my one-year research attachment at Center of Materials and Nanotechnologies (CEMNAT), University of Pardubice (UPCE). He is highly enthusiastic about science and committed to pushing the science boundaries forward. It is my great pleasure to work in his group, and I appreciate his guidance, advice and the rewarding learning experience during my stay. Sincere appreciation also goes to our collaborators from University of West Bohemia, Pilsen, Institute of Physics of the Czech Academy of Sciences, and Charles University, Prague.

I am thankful to my mentor, Dr. Hanna Sopha, for her helpful guidance in work, and my stay in UPa. I learn from her strong self-discipline and positive attitude. I enjoyed working with Dr. Raúl Zazpe, Dr. Miloš Krbal, Dr. Anitha Veettikkunnu Chandran, Dr. Filip Dvořák, Ing. Jan Přikryl, Ing. Luděk Hromádko and Dr. Veronika Podzemná. They have generously shared knowledge and facilitated me in many ways.

My genuine appreciation goes to Dr. Tneh Sau Siong and Dr. Beh Khi Poay, who were with me during my initial stage of study. I am fortunate to have Che Woei,

Yingqi, Lay Kim, Yuit Ling, Ing Khang, Zhi Yin and Pauline for their comradeship in the laboratory throughout my study years. Special thanks to Teng Yong, Pei Yen, Wei Hong and Chia Yon, who are in the academic field. I wish my friends every success in the new journey they are embarking.

Support from the technical team from School of Physics and Institute of Nano-Optoelectronics Research and Technology (INOR), Universiti Sains Malaysia (USM), Mr. Mohd Anas, Mr. Yushamdan, Mr. Abdul Jamil, Mr. Syed Mohammad, Mdm. Ee Bee Choo; as well as administrative and technical assistance from UPCE, Ing. Radka Přiklopilová, Mrs. Caroline Novák-Jolly, Mrs. Denisa Janebová are much appreciated.

This work is jointly funded by USM (Project no. 1001/PFIZIK/8011005), European Research Council (ERC, Project no. 638857) and Ministry of Youth, Education and Sports of the Czech Republic (Project no. LM2015082 and CZ.02.1.01/0.0/0.0/16_013/0001829). 'MyPhD' scholarship offered by Ministry of Education Malaysia is gratefully acknowledged. I am thankful for the research visit scholarship from UPa and USM. I am equally grateful for the conference fund for 1st ICASS 2015 at Shanghai by Institute of Postgraduate Studies USM, E-MRS Fall Meeting 2017 at Warsaw by ERC, 6th ICSSST 2017 Penang by School of Physics USM.

Finally, I am most indebted to my beloved parents for their unconditional love, infinite patience, and support over the years. I am grateful to my sister for taking care of the family during the days that I was away.

Words fail to convey my appreciation to each and everyone who has continuously supported, encouraged and motivated me to achieve the goal. Thank you.

TABLE OF CONTENTS

CHAPTER 4 – RESULTS AND DISCUSSION

LIST OF TABLES

LIST OF FIGURES

LIST OF ABBREVIATIONS

0D	Zero-Dimensional
1D	One-Dimensional
2D	Two-Dimensional
3D	Three-Dimensional
AAO	Anodic Aluminum Oxide
ALD	Atomic Layer Deposition
AO 7	Acid Orange 7
AR	Aspect Ratio
a.u.	Arbitrary Unit
CBD	Chemical Bath Deposition
CVD	Chemical Vapor Deposition
DC	Direct-Current
DRS	Diffuse Reflectance Spectra
DSSCs	Dye-Sensitized Solar Cells
EDTA	Ethylenediaminetetraaceticacid
EDX	Energy-Dispersive X-ray
e.g.	*Latin*: exempli gratia (for example)
EG	Ethylene Glycol
et al.	*Latin*: et alii (and others)
etc.	*Latin*: et cetera (and other things/and so forth)
FTO	Fluorine-doped Tin Oxide
FWHM	Full-Width at Half Maximum
HAADF	High Angle Annular Dark Field
HAR	High Aspect Ratio
ICDD	International Centre for Diffraction Data
i.e.	*Latin*: id est (that is)
IPCEs	Incident Photon-to-electron Conversion Efficiencies
ITO	Indium-Tin-Oxide
LbL	Layer-by-Layer

LED	Light Emitting Diode
LIBs	Lithium-ion Batteries
MB	Methylene Blue
MBE	Molecular Beam Epitaxy
MFC	Mass Flow Controller
MSM	Metal-Semiconductor-Metal
N/A	Not Available
PCB	Printed Circuit Board
PCE	Power Conversion Efficiencies
PEC	Photoelectrochemical
PLD	Pulse Laser Deposition
QD	Quantum Dot
RF	Radio-Frequency
Rh B	Rhodamine B
SAED	Selected Area Electron Diffraction
SCE	Saturated Caromel Electrode
SEM	Scanning Electron Microscope
SMU	Source Measuring Unit
STEM	Scanning Transmission Electron Microscope
TCO	Transparent Conducting Oxide
TEM	Transmission Electron Microscope
TMDCs	Transition Metal Dichalcogenides
TNTs	Titanium Dioxide Nanotubes
UV	Ultraviolet
VASE	Variable Angle Spectroscopic Ellipsometry
XPS	X-ray Photoelectron Spectroscopy
XRD	X-ray Diffraction

LIST OF SYMBOLS

α	Absorption coefficient
ε	Static dielectric constant
ε_0	Vacuum permittivity
λ	Wavelength
μ	Electron mobility
ν	Irradiation frequency
τ	Response time
ℓ	Length or distance of travel
d	Diameter of TiO_2 nanotube layer
d_{SC}	Width of space charge layer
C	Concentration of methylene blue
E	Electric field
E	Electric field
E_B	Binding energy
E_{FB}	Flat band potential
E_g	Band gap
f_g	Growth factor
h	Planck's constant
I	Ionic current
I_{ph}	Photocurrent
J	Photocurrent density
J_{SC}	Short-circuit current density
k	Photocatalytic decomposition rate constant
k_B	Boltzmann's constant
L	Thickness of TiO_2 nanotube layer
L_D	Debye length
m_o	Effective mass
n	Electronic transition
N_c	Carrier concentration

N_D	Donor density
P	Power density of irradiation light
q	Electron charge
$q\phi$	Energy barrier
R	Resistance
S	Sensitivity
T	Temperature
ΔU	Change of voltage
V	Applied potential
w	Wall thickness of TiO_2 nanotube layer

ZnO DAN $MoSe_xO_y$ PENGUBAHSUAIAN NANOTIUB TiO_2 UNTUK APLIKASI FOTO-ELEKTROKIMIA DAN PENDERIAAN

ABSTRAK

Lapisan anodik satu dimensi (1D) nanotiub titanium dioksida (TiO_2) yang tersusun sendiri telah menarik perhatian saintifik dan teknologi yang ketara selama lebih dari satu dekad. Kelemahan utama adalah jurang jalur yang agak lebar (3.0–3.2 eV) dengan foto-konduktiviti yang tinggi hanya dalam kawasan spektrum ultraungu (UV) ($\lambda \leq 390$ nm, $\approx$5% daripada spektrum suria), konduktiviti yang agak rendah dan kadar rekombinasi pembawa cas yang tinggi. Tambahan pula, sebagai nanostruktur bernisbah aspek tinggi (HAR), penciptaan salutan sekunder yang seragam dalam lapisan nanotiub TiO_2 masih merupakan satu cabaran. Untuk mengatasi isu-isu kritikal ini, kerja semasa adalah bertujuan (i) untuk menyintesiskan lapisan anodik 1D nanotiub TiO_2 sebagai semikonduktor berdikari dan untuk inkorporasi bahan-bahan sekunder; (ii) untuk sintesis lapisan ZnO dan $MoSe_xO_y$ yang homogen dan konformal dalam lapisan nanotiub TiO_2 dengan pemendapan lapisan atom (ALD); (iii) untuk membentuk heterostruktur bagi meningkatkan kecekapan pengangkutan caj, meningkatkan penyerapan cahaya dan memperluaskan julat berfungsi ke rantau spektrum cahaya nampak; dan (iv) untuk menilai tindak balas foto-pengesanan UV, tindak balas penderiaan etanol pada suhu yang rendah, penjanaan foto-arus dan foto-mangkin penguraian metilena biru (MB). Sintesis struktur nanotiub 1D TiO_2 dijalankan dengan penganodan elektrokimia konvensional bagi kepingan Ti dalam elektrolit organik yang berfluorin. Foto-pengesan UV yang bersifat pincang rendah dan tiada respon kepada cahaya nampak telah dibina dalam struktur berlapis yang terdiri daripada ITO/elektrolit/nanotiub TiO_2/Ti bagi kali pertama untuk menyiasat foto-pengesanan dalam rantau spektrum UV-A, B dan C. Ke-

pekaan tertinggi dikreditkan kepada lapisan TiO_2 5 μm, dengan kepekaan ≈850, responsiviti ≈ 740 mA/W dan masa kenaikan dan pemulihan yang cepat iaitu kurang dari 1.5 s. Kesan sinergi yang terhasil daripada bahan-bahan yang dipendap pada lapisan teras TiO_2 sangat mempengaruhi sifat-sifat foto-elektorkimia (PEC) dan meningkatkan kecekapan penukaran fotoarus dengan ketara. Lapisan nanotiub bersalut dengan ZnO (19 nm) membentangkan kecekapan penukaran foton-ke-elektron (IPCE) sebanyak 80-95% antara 305-375 nm dengan bantuan pincang 2 V. Nilai ini adalah antara nilai tertinggi yang dilaporkan untuk kombinasi ZnO/TiO_2. Lapisan yang bersalut dengan $MoSe_xO_y$ (2 nm) menunjukkan foto-arus sehingga 40 kali ganda lebih tinggi daripada lapisan nanotiub kosong fotoarus pada 470 nm. Untuk aplikasi alam sekitar, salutan $MoSe_xO_y$ telah ditunjukkan sebagai foto-mangkin yang berkesan untuk penguraian metilena biru (MB), dengan kadar penguraian foto-mangkin yang memecut pada 2.259×10^{-2} min^{-1}. Ini juga merupakan pada kali pertama, $MoSe_xO_y$ dihasilkan dengan ALD dan dimendapkan dalam nanostruktur HAR. Akhirnya, salutan ZnO menghasilkan tindak balas penderiaan etanol yang bertambah baik sebanyak 11 kali ganda berbanding dengan lapisan nanotiub kosong pada suhu operasi 100–200 °C dengan kestabilan, ketahanan, dan kebolehan pengulangan yang tinggi. Secara keseluruhannya, kerja terkini menunjukkan bahawa lapisan anodik nanotiub TiO_2 yang tersusun sendiri berfungsi sebagai lapisan penderiaan untuk pengesanan UV dan etanol; dan sebagai foto-mangkin dalam aktiviti PEC dan foto-uraian.

ZnO AND $MoSe_xO_y$ MODIFIED TiO_2 NANOTUBES FOR PHOTOELECTROCHEMICAL AND SENSING APPLICATIONS

ABSTRACT

One-dimensional (1D) anodic self-organized TiO_2 nanotube layers have attracted considerable scientific and technological interest over a decade. The major drawbacks are their rather wide band gap energies (3.0–3.2 eV) with high photoactivity only in the ultraviolet (UV) spectral region ($\lambda \leq 390$ nm, $\approx$5% of the solar spectrum), relatively low conductivity and high carrier recombination rate. Furthermore, as a high aspect ratio (HAR) nanostructure, the deposition of a uniform secondary coating within the TiO_2 nanotube layers remains a challenge. To overcome these critical issues, present work is intended (i) to synthesize anodic 1D TiO_2 nanotube layers as an independent semiconductor and for the incorporation of secondary materials; (ii) to produce homogeneous and conformal ZnO and $MoSe_xO_y$ coatings by atomic layer deposition (ALD) within TiO_2 nanotube layers; (iii) to form heterostructure in order to enhance charge transport efficiency, increase light absorption and extend the functional range to the visible spectral region; and (iv) to evaluate UV photodetection responses, ethanol sensing responses at low temperatures, photocurrent generation and photocatalytic degradation of methylene blue (MB). The synthesis of the TiO_2 nanotube layers was carried out by a conventional electrochemical anodization of Ti sheet in fluorinated organic electrolytes. A low bias, visible-blind, UV photodetector was constructed in a sandwich structure comprising of ITO/electrolyte/TiO_2 nanotubes/Ti for the first time to investigate the photodetection in UV-A, B and C spectral regions. The highest sensitivity was credited to 5 μm TiO_2 nanotube layer, with sensitivity $\approx$850, responsivity $\approx$740 mA/W and short rise and decay time less than 1.5 s. Synergistic effects arising

from the deposited materials and TiO_2 core layer strongly influenced the photoelectrochemical (PEC) properties and substantially enhanced the photocurrent conversion efficiencies. The ZnO (19 nm) coated nanotube layers presented 80–95% incident photon-to-electron conversion efficiencies (IPCE) between 305–375 nm with the aid of 2 V bias. This value is among the highest values reported for ZnO/TiO_2 combination. The $MoSe_xO_y$ (2 nm) coated layers demonstrated up to 40-fold higher photocurrent than the blank nanotube layers at 470 nm. As an environmental application, the $MoSe_xO_y$ coatings have shown to be an effective photocatalyst for MB degradation with significantly accelerated photocatalytic degradation rates at 2.259×10^{-2} min^{-1}. It is also for the first time, $MoSe_xO_y$ is synthesized by ALD and deposited within HAR nanostructure. Finally, the ZnO coatings yielded an improved ethanol sensing response up to 11-fold compared to the blank nanotube layers in operating temperatures of 100–200 °C with high stability, durability, and reproducibility. Overall, the current work demonstrated that anodic self-organized TiO_2 nanotube layer is functional as a sensing layer for UV and ethanol detection; and a photocatalyst in PEC and photodegradation activities.

CHAPTER 1

INTRODUCTION

1.1 Nanostructured materials

Nanostructured materials are low dimensional materials with physical dimension of 1–100 nm in at least one direction and demonstrate size effects [1, 2]. Nanomaterials possess a wealth of unique properties, including physical, chemical, electrical, optical and magnetic properties which are distinctly different from their bulk counterparts [3, 4]. Therefore, the miniaturization of a structure is more than mere advancement in reducing the physical size, but with remarkable modification to its properties [4]. In specific, the high surface-to-volume ratio of nanomaterials present large surface area, offer significantly more active surface sites to be in contact with solutions and gases (reactants) for higher reaction activities [5].

1.2 One-dimensional (1D) TiO_2 nanotube layer

One-dimensional (1D) nanostructures exist in diverse variants shown in Figure 1.1, which is categorized into two major forms, *i.e.* nanorods/nanowires and nanotubes. Nanorods and nanowires are very similar. However, nanowires possess a much higher aspect ratio in general. On the other hand, the most distinct difference between nanowires and nanotubes lies in the internal space of a tubular geometry which offers an additional active surface area as compared to a rod and wire of the same dimension.

The aspect ratio (AR) of a 1D nanostructure is defined as the ratio of the length to the diameter of a nanostructure [6, 7]. High aspect ratio (HAR) nanostructures such

as TiO_2 nanotubes further present remarkable light absorption and internal scattering properties (for further light absorption), thereby increasing the performance of light-driven applications [8–10].

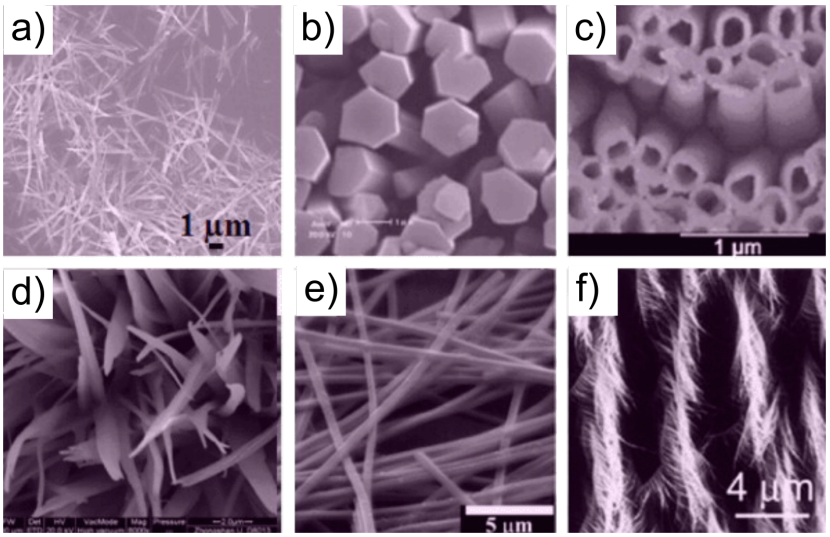

Figure 1.1: SEM images of 1D nanostructured materials in various forms (a) nanowires (b) nanorods (c) nanotubes (d) nanobelts (e) nanoribbons and (f) hierarchical nanostructures, adapted from Tiwari *et al.* [2].

1D geometry offers more superior charge collection efficiencies as compared to zero-dimensional (0D) nanoparticle or quantum dots (QDs). This is because the charge transport and collection process are strongly associated with the electrons and holes recombination rate and collection lifetime [5, 11]. Figure 1.2 illustrates the charge separation and transport behavior of 0D and 1D electrodes. Nanoparticulate and mesoporous layers are not preferred as the trapping states at the grain boundaries cause comparably longer diffusion paths [5, 11]. For well-aligned 1D structures such as nanorods and nanotubes, the charge transport follows the direct pathway along the structures to the substrate that acts as back contact [12]. For example, the electron-hole pairs recombination time of 1D TiO_2 nanotube layer is 10 times slower than that of 0D TiO_2 nanoparticle layer and yields 25% higher charge collection efficiency [9].

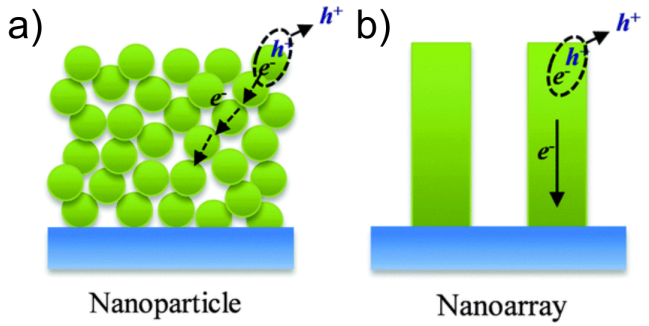

Figure 1.2: Schematic comparison of (a) 0D and (b) 1D photoelectrodes charge separation/transport behaviors, adapted from Chen *et al.* [11].

Based on the above reasons: (i) high specific surface area, (ii) rapid charge transport and (iii) strong light absorption and internal scattering, hence, TiO_2 nanotube layer is preferred in this work. Through electrochemical anodization, a TiO_2 nanotube shown in Figure 1.3(a) grows perpendicularly on the surface of a Ti metal (details of the growth will be described in Section 2.3.1). When plenty of these single nanotubes simultaneously self-organizes on the Ti surface, a well-aligned oxide layer resembling a layer of film is formed as illustrated in Figure 1.3(b). Therefore, this structure is known as the anodic self-organized TiO_2 nanotube layer.

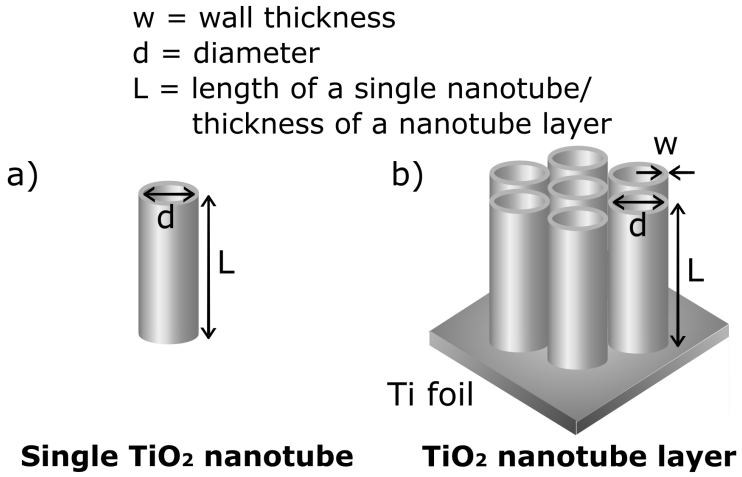

Figure 1.3: Schematic diagram of (a) a single TiO_2 nanotube and (b) a layer of TiO_2 nanotube.

As a wide band gap semiconductor, TiO_2 has discovered its scientific purposes in

energy applications, notably photoelectrochemical (PEC) water splitting by Honda and Fujishima [13] and Grätzel solar cells [14]. In addition, TiO_2 is a promising material in photocatalytic environmental purification, reduction of CO_2, direct methanol fuel cells, microbiocide, hydrophilic for anti-fogging and self-cleaning, ion-intercalation batteries and supercapacitors, resistive switching memory, drug delivery implants, physical and chemical sensors [15, 16].

1.3 Heterostructure and heterojunction

Semiconductor heterostructure is formed by a combination of two or more semiconductor materials, and a heterojunction is an interface between the two layers in contact. The heterojunction can be categorized into three types as shown in Figure 1.4 [17, 18].

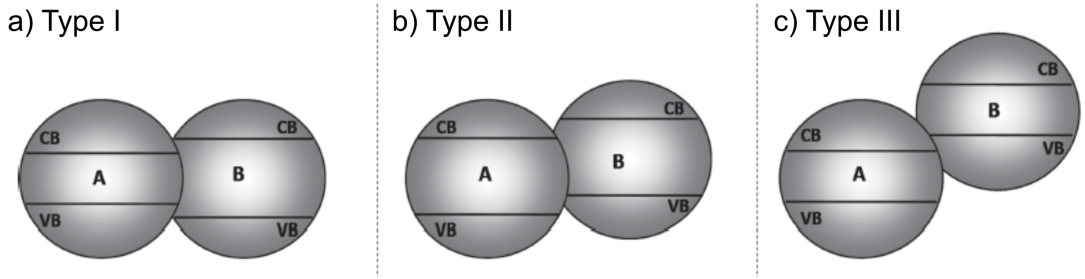

Figure 1.4: Schematic representation of the types of heterojunction formed by two semiconductor materials (a) type I - straddling gap, (b) type II - staggered gap and (c) type III - broken gap. CB and VB denote the conduction and valence band of semiconductor (A and B), respectively, adapted from Marschall [17].

Among the three types of heterojunction, type II with staggered gap presents the optimal band positions. The CB edge and VB edge of one material (B) is higher than the other (A) which creates an energy gradient at the interface of A and B. The photoexcited electrons are transferred from CB (B) to CB (A) whereas the holes are transferred

in the reverse direction from VB (A) to VB (B). The electrons transfer is related to the favorable band positions and band bending at the interface due to the internal electric field [17–19]. Efficient separation of the photogenerated electrons and holes, reduction of the recombination rate and prolongation of the electron lifetimes are achieved within this scheme [17–19]. Hence, the heterostructure of two semiconductor materials is often designed based on this type II heterojunction, including the modifications of TiO_2 nanotube layers in this work.

1.4 Problem Statements

Anodic self-organized 1D TiO_2 nanotube layers present a fascinating, highly-ordered structure which has been extensively investigated for their morphology, crystallinity and other properties in relation to its adjustable fabrication conditions [12, 20]. However, as a functional semiconductor, the major drawbacks of TiO_2 nanotube layers are

i. their rather wide bandgap energies (3.0–3.2 eV) with high photoactivity only in the UV spectral region ($\lambda \leq 390$ nm), equivalent to $\approx$5% of the solar spectrum – limitation in photon absorption for PEC and photocatalytic degradation.

ii. their relatively low conductivity and high charge carrier recombination rate of the photogenerated electron-hole pairs – inefficient charge transport (quantity, speed) for any semiconductor applications.

iii. their HAR morphology to produce a uniform coating adhering the wall of the tubes, particularly to achieve the bottom of the nanotubes without overfilling and obstructing the surface of the tubes – challenge to develop an efficient heterojunction with a secondary material.

1.5 Research motivations

Although the TiO_2 nanotube layers have been long studied in many light-driven applications [12, 20–23], it has not been a popular choice for PEC ultraviolet (UV) photodetector. Positive UV light detection results based on solid-liquid heterojunction photodetector were primarily based on TiO_2 nanorods fabricated by hydrothermal reactions on fluorine-doped tin oxide (FTO) substrate [24–28]. Unlike the solid-state photodetector which requires high bias, commonly 5–30 V [29–36] to prevent the recombination of the photogenerated electron-hole pairs, the operation of solid-liquid detector demands only low driving voltage or even self-powered by the structure itself. The demand for monitoring the exposure or dosage of UV radiation in diverse fields have been increased over time, as solar or synthetic UV radiation sources have been widely utilized in military and civilian applications, such as astronomy, outer space communication, flame detection, memory storage, optoelectronic circuits, remote control, biological analysis, food industry and environmental disinfection [24, 37–42]. Excessive exposure to these UV sources is deleterious and may cause adverse health effects, for instance, premature aging, erythema, cataracts, skin cancer, melanoma, carcinogenesis and mutagenesis [38, 43, 44].

To resolve the core issues of TiO_2 nanotube layers described in Section 1.4, *i.e.* to reduce the charge carriers recombination rate and to increase the light harvesting efficiencies [45, 46], tremendous efforts have been devoted to modify the nanotube layers. This includes band gap engineering though transition metal [47, 48] and non-metal [49–51] dopings, as well as the introduction of a secondary material [52–62] to form a composite or heterostructure with TiO_2. All these works are to reduce the band

gap energy of TiO_2, broaden its optical absorption to the visible spectral region, so as to harness more energy from the abundant solar energy source [46–51].

Among the many attempts to incorporate another material within the TiO_2 nanostructures, metal oxides nanostructures (*e.g.* WO_3 [56], SnO_2 [63], CuO [64], NiO [65], Al_2O_3 [66], In_2O_3 [67], and ZnO [68, 69]) turn out to be suitable to form p-n or n-n junctions at the interface with TiO_2 to alter the band structure. Out of these, ZnO offers high electron mobility for fast charge transport and low carrier recombination rate, and both ZnO and TiO_2 have close band gap energies (3.37 and 3.0–3.2 eV, respectively) [70, 71]. Since both materials complement in properties, many works have coupled ZnO and TiO_2 to form a new heterostructure [54, 68–75].

The advantages of ZnO-TiO_2 heterostructures include the suitable energy level alignment between ZnO and TiO_2, suppression of unwanted electron-hole recombination, shift in band gap energy, and hence extension of the operational range in the visible spectral region [72–74]. These effects have been efficiently utilized for a high photocatalytic activity including H_2 production [54], photocatalytic degradation of organic dyes [52, 53, 73–77] and dye-sensitized solar cells (DSSCs) [69, 78]. Advantages of the TiO_2/ZnO heterostructure can also be exploited for chemical sensing applications. An improved sensing performance is associated with band bending due to Fermi level equilibration, reaction sites enhancement and synergistic reactions effect [79–81]. Moreover, the sensitivity is maximized if the sensing layer is fully depleted, that is, if the nanostructure dimension is comparable to the electron depletion layer [80, 82].

There are numerous approaches to integrate ZnO within TiO_2 nanostructures, such as chemical bath deposition (CBD) [54], dip-coating [72], sputtering [75], hydrothermal reactions [81], layer-by-layer (LbL) assembly [83] and atomic layer deposition (ALD) [68, 69]. However, only ALD produces conformal and homogeneous deposition of a thin layer of material, with precise control of the coating thickness according to the deposition cycles [84]. The peculiar characteristics are particularly helpful for the deposition of a secondary material in HAR structures, *i.e.* TiO_2 nanotube layers, in this study. Previous research has shown the potential of ALD secondary material in TiO_2 nanostructures [67–69, 77, 79, 80, 85–90]. These include ALD ZnO loaded 1D TiO_2 nanowires and nanotubes, mainly focused on the photocatalytic and PEC applications [68, 69, 77, 86]. However, gas sensing application based on ALD prepared TiO_2/ZnO heterostructure are limited. Up to now, only hydrothermally grown TiO_2 nanorods with ALD ZnO shell have been applied for detection of low concentration ethanol at 150 °C [79], and ALD double-layer TiO_2/ZnO hollow fibers for improved detection of CO gas [80]. Nevertheless, the reported well-aligned or highly ordered TiO_2 core nanostructures were in the thicknesses of 0.5–2.3 μm [68, 69, 77, 79, 86], which possessed limited surface area for light-induced photoactivity and efficient sensing. Thus, it is beneficial to explore uniform ZnO coatings from the surface to bottom of HAR TiO_2 nanotube layers.

The combination of two materials complements their individual properties and presents synergetic effects for different applications [91]. To maximize the positive synergies from two materials, utilization of tailored nanoscale architectures is desirable to increase the surface area for reactions and prolong the photogenerated charge carriers lifetime [77, 92]. In this regard, core-shell structure is captivating for its intimate

contact between two layers helping to facilitate the charge separation by transferring photoelectrons from the shell to core layer [91, 92], possessing a staggered type energy band alignment between two materials [93, 94], as well as reduced band gap energy of the entire nanostructure by the narrow band gap shell layer [94].

For a material with small and tunable band gap, eminent photoactivity in the visible spectral region yet retains excellent electronic properties, such as high electrical conductivity, which cannot be realized by other semiconductor nanostructures [95, 96]; an exciting class of material *i.e.* two-dimensional (2D) transition metal dichalcogenides (TMDCs) emerge as promising prospects in light-driven applications. More recently, TMDCs have been integrated with TiO_2 structures for photocatalysis applications [93, 97–106]. The neighboring layers of TMDCs are bonded together by weak Van der Waals forces, thereby allowing the incorporation of two materials without lattice mismatch constraints [95]. However, the formation of TMDCs by ALD on a substrate is accompanied by the creation of a strong covalent bond. A number of MoS_2 or WS_2 coupled with TiO_2 composites or heterostructures have been reported for enhanced photocurrent conversion efficiency [97, 107], photocatalytic water splitting [98–100, 108], and photocatalytic degradation of organic pollutants [101, 103, 104, 106, 109], carried out in the UV and visible spectral region. In comparison, limited reports are available on another TMDCs member, $MoSe_2$, integrated with TiO_2 [93, 105], although there are a number of studies utilizing MoO_3–TiO_2 [59–61]. Nevertheless, visible light photocatalytic reduction of Cr(VI) to Cr(III) [93], photocatalytic degradation of Rhodamine B (Rh B) [55, 61], acid orange 7 (AO 7) [60] and methylene blue (MB) [105], indicate that the introduction of MoO_3 or $MoSe_2$ within TiO_2, or vice versa, can lead to significantly enhanced degradation rates. In addition, a

combination of different group of materials for new transition metal compounds, such as molybdenum oxysulfides [110], oxyselenides [111] and sulfoselenides [112] have been introduced to investigate their unknown properties. Therefore, it is interesting to explore the modification of TiO_2 nanotube layers by these materials.

1.6 Research objectives

Present work aims

i. to prepare anodic self-organized 1D TiO_2 nanotube layers of different dimensions according to the optimization from previous recipes for UV photodetection and deposition of secondary materials.

ii. to enhance the charge transport efficiency, increase light absorption and extend the functional range of TiO_2 nanotube layers to the visible spectral region by creating a heterostructure with secondary materials.

iii. to produce uniform and conformal secondary ZnO and $MoSe_xO_y$ coatings of different thicknesses from top to bottom within HAR TiO_2 nanotube layers by ALD.

iv. to assess the performance of the blank and secondary materials modified TiO_2 nanotube layers for (i) UV photodetection in a PEC cell, (ii) ethanol sensing response at low temperatures, (iii) photocurrent generation and (iv) photocatalytic degradation of MB.

1.7 Originality

Novel or renewed knowledge derived from this work, are summarized as follows.

i. Integration of anodic self-organized TiO_2 nanotube layers as sensing layer, for

the first time, in a small, light-weight and portable prototype PEC cell as solid-liquid heterojunction UV photodetector. This cell requires low driving voltage, yet demonstrates fast response and recovery times $<$1.5 s and high sensitivity $\approx$850, high responsivity $\approx$740 mA/W in the UV-A region.

ii. Conformal secondary coatings from top to bottom within HAR 5 μm TiO_2 nanotube layers by ALD for ZnO and $MoSe_xO_y$ coatings.

iii. Deposition of homogeneous layer of ZnO within the anodic TiO_2 nanotube layers (i) Extended photo-active region to 420 nm, and photocurrent generation assisted by external bias recorded up to 8-fold enhancement, equivalent to $\approx$95% IPCE in the UV spectral region, among the highest in the literature for ZnO/TiO_2 combination. (ii) Improved ethanol sensing response up to 11-fold at the operating temperature 200 $^{\circ}$C with excellent stability and reproducibility.

iv. First deposition of ultrathin and uniform $MoSe_xO_y$ coatings by ALD within the anodic TiO_2 nanotube layers. (i) Improved photocurrent generation at UV (365 nm) and visible spectral region (470 nm) by 4- and 40-fold, respectively. (ii) Accelerated photocatalytic degradation rate of MB, up to 75-fold, all in reference to the uncoated nanotube layers.

1.8 Organization of thesis

This thesis is divided into five chapters. A brief introduction to this thesis, problem statements, research motivations, objectives and originality are given in Chapter 1.

Chapter 2 reviews the fundamental properties and the background of TiO_2. Growth mechanisms of anodic self-organized TiO_2 nanotube layers, major factors which influ-

ence the structural and morphological properties, as well as some major breakthroughs in the history of TiO_2 nanotube layers are included. Subsequently, modification of the nanotube layers by different techniques and secondary materials including metals, oxides and chalcogenides for improved performance are discussed. Furthermore, the background and principles of ALD, deposition of secondary materials by ALD within nanotube layers are critically reviewed. Lastly, vast practical applications as photocatalysts in PEC and degradation activities, photodetector and chemical sensors are discussed. The working principles and some critical examples are included.

Chapter 3 describes the preparation of TiO_2 nanotube layers through electrochemical anodization and subsequent integration of ZnO and $MoSe_xO_y$ coatings through ALD. Characterization equipment and the applied settings are concisely stated. In addition, details of UV photodetection, PEC activity, photocatalytic degradation of organic dye (MB), and chemical (ethanol) sensing measurements are provided.

Chapter 4 reveals the physical properties of the blank TiO_2 nanotube layers for UV sensing response and discusses the sensing mechanism. Next, the physical properties of the secondary materials (ZnO and $MoSe_xO_y$) modified TiO_2 nanotube layers are presented. The performance of these modified nanotube layers in PEC activity, photocatalytic degradation of MB and ethanol sensing are discussed. The enhanced performance in the mentioned applications by the modified nanotube layers are elucidated and compared with the works in literature.

The final chapter, Chapter 5 concludes the major findings and completes the thesis with future directions which can be developed from the present work.

CHAPTER 2

LITERATURE REVIEW

2.1 Introduction

This chapter provides an overview of the fundamental properties of TiO_2. The research background of TiO_2 and important developments in anodic self-organized TiO_2 nanotube layers are reviewed. Subsequently, the incorporation of secondary material within the hollow interior of the nanotube layers are comprehensively evaluated. These secondary materials include metal nanoparticles, oxides, sulfides, selenides nanostructures prepared by different approaches, in particular, the modification by atomic layer deposition employed in this work. Finally, the applications of these modified TiO_2 nanotube layers in photoelectrochemical and sensing activities are surveyed.

2.2 Titanium dioxide (TiO_2) and TiO_2 nanotube layers

2.2.1 Properties of TiO_2

Titanium dioxide, TiO_2, also known as titania, is abundant, non-toxic and chemically stable. It is a wide band gap n-type semiconductor with high refractive index, determined by its crystalline polymorphs, namely, anatase, rutile, and brookite. These crystal structures consists of distorted TiO_6 octahedral in different manners as depicted in Figure 2.1 [113, 114]. The different crystalline phases thereby possess different physical properties, and an overview is given in Table 2.1. Among the three crystalline polymorphs, rutile is the most common form in nature and is thermodynamically stable, but anatase is recognized as a better photocatalyst than rutile in several aspects

[115]. In fact, anatase (≈3.2 eV) possesses a larger band gap than rutile (≈3.0 eV) which comparatively does not favor the light absorption. However, comparing the indirect band gap of anatase and direct band gap of rutile, the indirect band gap offers slower charge recombination rate, hence, longer charge carrier lifetime promotes more surface reactions between TiO_2 and molecules [116].

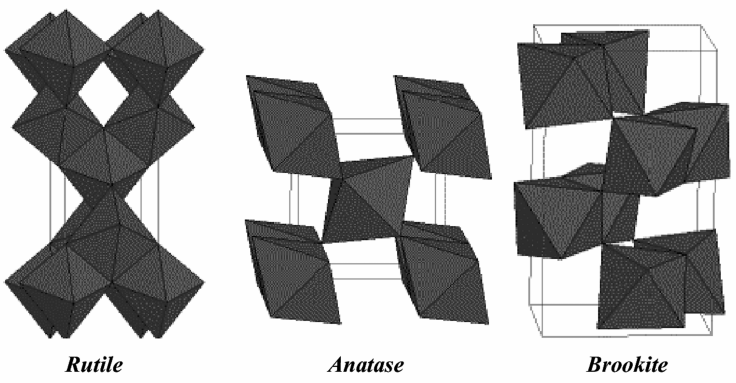

Figure 2.1: The different polymorphs of TiO_2, adapted from Dambournet *et al.* [117].

For surface reaction, the interaction of molecules with TiO_2 surface depends on the adsorption of molecules and charge transfer. These factors are affected by the properties such as surface orientation, polymorph, surface defects, electronic structure, and potential differences (work function and flat band potential related) [118, 119]. For charge transfer, excitons possess a preferred diffusion direction along specific orientation, and travel to the surface within its lifetime for efficient reaction with surface molecules. This can be further related to the excitons mobility, measured by effective mass, m_o. Anatase is reported to have a lower effective mass of $\approx m_o$ than rutile of ≈7–8 m_o [119]. Based on the several advantages in the literature, anatase TiO_2 was adopted in this work, where the as-grown TiO_2 nanotube layers in amorphous form were crystallized to anatase on purpose through calcination in specific conditions, which will be described in Section 3.2.2.

Table 2.1: Physical properties of anatase, rutile and brookite TiO_2 at room temperature [113, 120–130].

	Anatase	Rutile	Brookite
Molar mass (g/mol)	79.890	79.890	79.890
Formula units/cell (Z)	4	2	8
Crystal system	Tetragonal	Tetragonal	Orthorhombic
Point group	4/m 2/m 2/m	4/m 2/m 2/m	2/m 2/m 2/m
Space group	D_{4h}^{19}-$I4_1$/amd	D_{4h}^{14}-$P4_2$/mnm	D_{2h}^{15}-Pcab
Unit cell (Å)	a = 3.7845	a = 4.5937	a = 5.4558
	b = N/A	b = N/A	b = 9.1819
	c = 9.5143	c = 2.9587	c = 5.1429
Volume ($Å^3$)	136.25	62.07	257.38
Molar volume (m^3/mol)	20.156	18.693	19.377
Density (g/cm^3)	3.895	4.2743	4.123
Refractive index	≈2.5	≈2.8	≈2.6
Band gap energy (eV)	3.2–3.4	3.0–3.2	3.1
Work function (eV)	≈5.1	≈4.9	≈4.3
Resistivity (Ω.cm)	$1–10^{-4}$	$1–10^{-4}$	$10^{-1}–10^{1}$
Mobility (cm^2/V.s)	$10^{-1}–10^{1}$	$10^{-1}–10^{1}$	$10^{1}–10^{2}$
Carrier concentration (cm^{-3})	$10^{17}–10^{19}$	$10^{17}–10^{19}$	$10^{16}–10^{19}$

2.2.2 Background of TiO_2

The pioneering work of Fujishima and Honda [13] in 1972 on the photoelectrochemical (PEC) water splitting utilized TiO_2 anode as a photocatalyst to decompose water into hydrogen and oxygen, in an effort to develop a clean and renewable energy source, which potentially resolves environmental issues and energy crisis in near future [131]. Since then, TiO_2 is regarded as the key photocatalytic material, with more than thousands of journal articles published to date [45]. The principle is based on the semiconductor nature of TiO_2, when UV light (or irradiation source greater than the band gap of TiO_2) is absorbed, electron-hole pairs are generated for reduction/oxidation (redox) reactions with the environment [131].

Apart from the generation of H_2 and O_2 gases, photocatalysts can be extended to other applications such as reduction of CO_2 to methane, methanol and formic acid, and oxidation of organic pollutants [16, 132]. The early work on the irradiation of TiO_2 for purification of water via photocatalytic degradation of pollutants was demonstrated by Frank and Bard in late 1970s [45, 133, 134]. These initial works and many reports later have shown that photo-oxidation of inorganic and organic contaminants is a promising route for environmental remediation [47, 135–140].

Another widely investigated application of TiO_2 is the Grätzel-type dye-sensitized solar cells (DSSCs) developed by O'Regan and Grätzel in 1991 [14], which is reportedly the first fully functional solar cell with solar light conversion efficiency up to 12%. This groundbreaking work employed TiO_2 nanoparticles as photoanode, with Ru complex dye as a light absorber, sandwiched by a platinized transparent conductive oxides (TCO) as cathode [14]. DSSCs was sought as an alternative to the conventional solid-state photovoltaic technology [141, 142], however, due to certain drawbacks, it never really turned into a competitive and viable commercial photovoltaic solution. To date, the highest efficiency for DSSCs is recognized as 13% at full sun illumination, by $[Co(bpy)_3]^{2+/3+}$ redox couple with porphyrin sensitizers SM315 [143].

These series of works have stimulated the continuously growing interest in the materials science community to pursue highly efficient TiO_2 photocatalysts through numerous design and modifications of materials [144]. TiO_2 has been long studied and recognized as the most promising photocatalyst, owing to its non-toxicity, relatively low-cost synthesis, chemical inertness, and resistance against photocorrosion [46, 145, 146]. Thus, various techniques to synthesize metal oxides nanomaterials have been

adopted to prepare TiO_2 nanostructures. Among all, sol-gel, hydrothermal reactions and electrochemical anodization are notably the more popular approaches [15, 147].

The idea derived from sol-gel processing method is to dissolve one or more compounds in a solvent and then restore in solid form. It is widely applied to prepare thin films, powders, pores and fibers [148]. In order to form ordered TiO_2 nanorods or nanotubes, this method is extended to a template, typically anodic alumina oxide (AAO) porous layers. After the sol-gel deposition, the template is easily dissolved in aqueous H_3PO_4 [149, 150] or NaOH [151] to obtain the TiO_2 nanostructures. The resultant rod or tube morphologies such as density distribution, length, and diameter, are predominantly dependent on the dimension of the templates. The crystalline phases of TiO_2 is refined during the final stage of the heating process, where lower temperatures yield anatase phase whereas elevated temperatures produce rutile phase [152]. The template-assisted method can be applied to other deposition techniques such as electrodeposition [153], ALD [29, 154, 155], with partial filling of the AAO porous layers to obtain TiO_2 nanotubes [29, 154, 155].

In 1998-1999, Kasuga *et al.* introduced alkaline hydrothermal reactions to synthesize TiO_2 nanotubes [156, 157]. The anatase or rutile TiO_2 powder is treated in aqueous NaOH and centrifuged to form Ti-OH bond in sheet-like structure. A post acid treatment dehydrates the Ti-OH bond to Ti-O-Ti bonds (shorter bond distance), leads to the folding of the sheet to form a tubular TiO_2 structure [157]. This method was then modified to grow standing rutile TiO_2 nanorods usually on fluorine-doped tin oxide (FTO) substrate. Titanium n-butoxide, titanium isopropoxide or titanium tetrachloride are frequently used as Ti precursor [76, 158]. A sol-gel spin-coated or

sputtered TiO_2 film may serve as seed layer to facilitate the growth, orientation, and dimensions of the resulting hydrothermally grown TiO_2 nanorods [159, 160].

Conversely, electrochemical anodization is simple and straightforward, does not require a sacrificial template, or a seed layer to produce well-aligned, highly-ordered, self-organized TiO_2 nanotube layer. Therefore, over the last thirteen years, anodization appears as the most studied technique to prepare a TiO_2 nanostructure. It has been pointed that the study of anodic 1D TiO_2 nanotube layers is growing exponentially, with various modifications such as doping, decoration, and functionalization for practical applications [12].

2.3 Synthesis of self-organized TiO_2 nanotube layers

2.3.1 Electrochemical anodization – Growth of TiO_2 nanotube layers in fluoride electrolytes

A conventional electrochemical anodization cell is shown in Figure 2.2. Here, the classical anodization of titanium which is also applicable to any valve metals in acidic or alkaline solutions (F^- ions free electrolyte) is described. When sufficiently high external potential is applied, at anode, Ti is oxidized to Ti^{4+} (Equation 2.1), (i) to form metal oxide, TiO_2 (Equation 2.2) or (ii) Ti is solvatized and dissolved in the electrolyte, Ti^{4+}_{solv} (Equation 2.3). At cathode, deprotonation liberates H_2 gas (Equation 2.4) [12, 20, 23].

$$Ti\ (s) \rightarrow Ti^{4+}\ (aq) + 4e^- \tag{2.1}$$

$$Ti\ (s) + 2H_2O\ (l) \rightarrow TiO_2\ (s) + 4H^+ + 4e^- \tag{2.2}$$

$$Ti^{4+}\ (aq) + solv \rightarrow Ti^{4+}_{solv}\ (aq) \tag{2.3}$$

$$2H^{+} + 2e^{-} \rightarrow H_2\ (g) \tag{2.4}$$

When classical electrolytes are employed to anodize Ti, the oxide (TiO_2) formed is insoluble, and the formation of oxide layer predominantly follows the reaction described in Equation 2.2. Subsequent thickening of the oxide layer is contributed by field-aided ion migration of O^{2-} and Ti^{4+} ions, influenced by the ionic current, I, described in Equation 2.5.

$$I = A\ \exp(BE) = A\ \exp\left(\frac{B\Delta U}{L}\right) \tag{2.5}$$

where ΔU is the voltage across the oxide, E is the electric field and L is the layer thickness, A and B are constants.

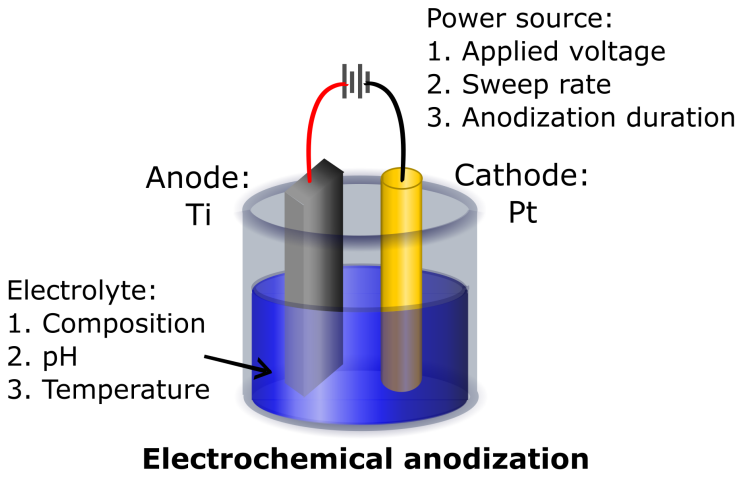

Figure 2.2: Conventional electrochemical anodization setup and the controllable anodization parameters.

In the presence of F^{-} ions, the growth of oxide layer is due to (i) formation of water-soluble $[TiF_6]^{2-}$ complex ions (Equation 2.6) and (ii) small ionic radius of F^{-} enter the growing TiO_2 oxide layer to be transported by applied electric field and com-

pete with the transport of O^{2-}. The formation of complex ions attacks (dissolution) of the formed TiO_2, and prevents $Ti(OH)_xO_y$ precipitation during the solvatization of Ti^{4+} ions to fluoride-complex $[TiF_6]^{2-}$ (Equation 2.7), prior to the reaction with precipitated $Ti(OH)_xO_y$ [12, 20], depicted in Figure 2.3.

Chemical dissolution of the oxide as soluble fluoride-complex is given by Equation 2.6, whereas direct complexation of high-field transported cations (Ti^{4+}) at the oxide/electrolyte interface is described in Equation 2.7.

$$TiO_2\ (s) + 6F^-\ (aq) \overset{H^+}{\rightarrow} [TiF_6]^{2-}\ (aq) + 2H_2O\ (l) \tag{2.6}$$

$$Ti^{4+}\ (s) + 6F^-\ (aq) \rightarrow [TiF_6]^{2-}\ (aq) \tag{2.7}$$

Overall, the formation of tubular TiO_2 under the influence of F^- is a competition between solvatization and oxide formation. Optimization of these two reactions and the establishment of steady-state current results in well-defined tubular structure [12, 20, 23].

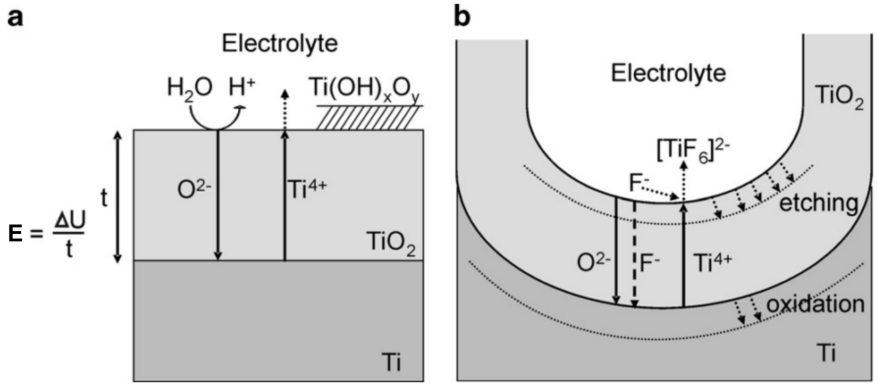

Figure 2.3: Schematic illustration of the anodization of Ti (a) compact oxide layer and (b) tubular oxide layer (with the influence of F^- ions), adapted from Macak *et al.* [20].

2.3.2 Structural and geometrical influence

Despite F^- ions being the key component of tube formation, in an electrochemical process, other parameters namely the anodization potential, duration, and electrolyte (composition, pH, temperature) strongly affect the geometry of the TiO_2 nanotube layers, such as pore diameter, wall thickness and nanotube layer thickness. Overall, the influence of the anodization parameters on the morphologies of tube layers is summarized in Figure 2.4. For a complete picture on the influence of anodization conditions towards the growth of the nanotube layers, the readers may refer to several excellent review articles [12, 20, 147, 161, 162].

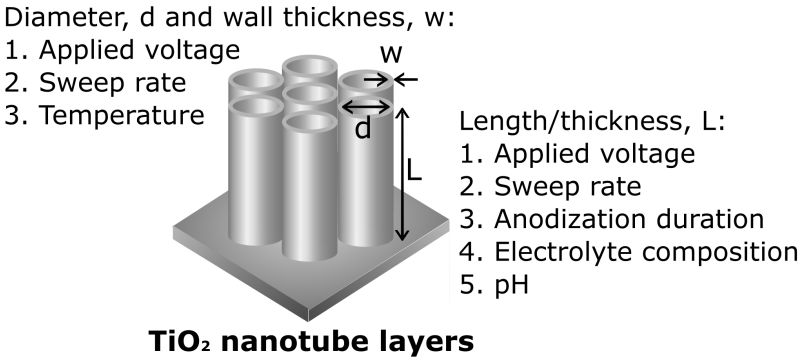

Figure 2.4: The major influences on the geometry of TiO_2 nanotube layers according to the controllable anodization parameters.

2.3.2(a) Anodization potential

The applied potential governs the pore/tube diameter and the thickness of an oxide layer. A higher anodization potential creates a stronger electric field which accelerates the formation of pits on the metal surface. Therefore, the increased number of pits further excavates to form a larger cavity, and larger diameter tubes were produced [163, 164]. To form a well-defined tubular structure, a minimum electric field (threshold voltage) is required to achieve the dissolution of the oxide layer in a F^- electrolyte

whilst maintaining the formation of the oxide during the anodization process. Beneath a certain potential, network-like porous structure is observed [165–168]. It has been proposed that the tube diameter, d is related to anodization potential, V by d = k $\times$ V, where the constant k = $2f_g$, and f_g is the growth factor for anodic oxides, and for TiO_2, $f_g \approx 2.5$ nm/V [20]. Furthermore, a higher anodization potential promotes the transport of the ionic species to the barrier layer of TiO_2/Ti. The higher dissolution rate at the barrier layer translates into higher deepening rate of the nanotubes to form longer tubes (thicker tube layer) [163, 169].

2.3.2(b) Anodization duration

Anodization duration is a key factor to determine the thickness of the TiO_2 nanotube layers. The growth rate in an aqueous electrolyte is higher than in an organic electrolyte. In other words, within the same duration, longer tube (thicker tube layer) is obtained in an aqueous electrolyte. Nevertheless, the overall trend follows that prolonged anodization extends the duration of steady-state current (see Section 2.3.1), and allows the growth of thicker oxide layer [23]. Up to a point, saturation of oxide growth was recorded [170], and once exceeds the oxide dissolution, a reverse effect was recorded [171].

2.3.2(c) Composition of electrolyte

In 1984, the pioneering work on self-organized TiO_2 nanotube layers by Assefpour-Dezfuly *et al.* [172] in chromic acid-based electrolyte and later by Zwilling *et al.* [173] in HF + chromic acid electrolyte, reported nanotube layers of thickness less than 500 nm. Such recipe was then modified by Gong *et al.* where the anodization was con-

ducted in 0.5 wt% HF + water [165]. These initial works demonstrated that F^- ions is the essential component in the formation of tubular structure. The anodic TiO_2 nanotube layers obtained from the aqueous electrolytes showed considerable inhomogeneity, in specific, the tubes were not closely connected to the neighbor tubes and the walls were rough with apparent ripples [174]. Many works have been carried out to improve the morphologies through varying the cationic species of F^- [175] and acids [176], introducing oxidizing agents [177], adding buffered components [178–180] and polar organic components [171, 181] in the electrolyte.

Crucial improvement on the morphologies of TiO_2 nanotube layers was demonstrated by Macak *et al.* [182] by introducing a high viscous electrolyte, *i.e.* glycerol and ethylene glycol. For the first time, very smooth tube walls up to 7 μm with near-ripple-free walls were well connected to the neighbor tubes. A distinguished appearance between the aqueous and glycerol-based electrolyte tube layers is seen in Figure 2.5. This is ascribed to the much lower current density in high viscosity electrolyte, so that the current fluctuations during the anodization process were inhibited [182, 183]. As a result, steady-state current over a long period of time favors the growth of smooth nanotubes. Since the growth rate in organic electrolytes is lower, anodization durations may be extended to allow the growth of thicker layer. Following this major breakthrough, high aspect ratio, self-organized TiO_2 nanotube layers up to few hundred microns were achieved under optimized anodizations [184, 185].

To accelerate the growth rate, chelating agents ethylenediaminetetraacetic acid (EDTA) [187, 188] and lactic acid [189] have been added to the electrolyte. EDTA captures Ti^{4+} ions to form Ti(EDTA) and TiO(EDTA) while releases F^- ions from

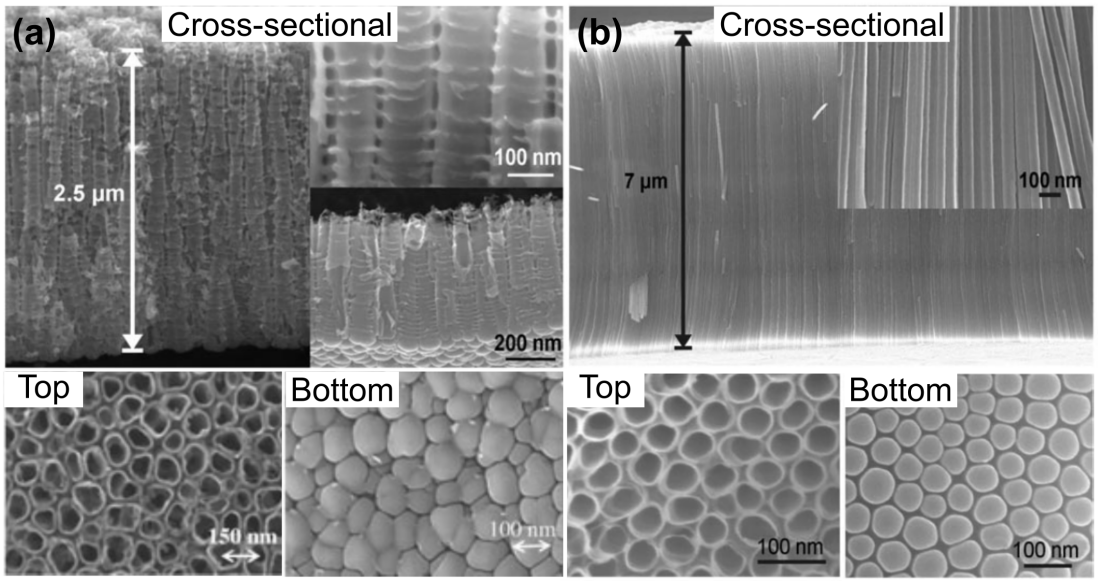

Figure 2.5: SEM images for the comparison of TiO_2 nanotube layers, cross-sectional, top and bottom (oxide/Ti substrate interface) views, produced in (a) aqueous-based and (b) glycerol-based electrolyte, adapted from Macak *et al.* [182, 186].

$[TiF_6]^{2-}$ complex. The released F^- ions then further react with TiO_2 and generate more $[TiF_6]^{2-}$ and increase the dissolution of the formed TiO_2, in turn accelerate the growth rate (see Section 2.3.1 for formation mechanism). With the aid of EDTA and lactic acid in ethylene glycol electrolytes, ultrahigh growth rates ≈27–41 μm/h [187, 188] and ≈20 μm/min [189], respectively were attained. These growth rates are unprecedentedly higher than the conventional growth rates, typically few-μm/h [170, 171, 177, 183, 190, 191].

2.4 Secondary material within TiO_2 nanotube layers

2.4.1 Overview

Combination of two materials such as hybrid materials combine the properties from the individual constituents, yielding synergistic effects, better properties for higher performance in applications as compared to their individual constituents. The reasons to incorporate a secondary material within TiO_2 nanotube layers may be categorized

into four major points as follows.

i. **Modification of surface chemistry.** The electron traps or recombination centers on the surface of TiO_2 nanotubes can be annihilated by a high quality or defect-free coating along the tube walls [77, 90] to enhance the photo-generated charge carrier separation [192–194]. An ultrathin secondary layer such as ZnO [68, 77, 195] and Al_2O_3 [196–198] in nanometer thickness is sufficient to passivate the tube walls.

ii. **Formation of semiconductor heterojunction.** *i.e.* n-n or p-n junction, with the n-type TiO_2 nanotube layers, particularly type-II staggered gap heterostructure [199, 200]. The favorable conduction and valence band edge positions of the two materials create an energy gradient at the interface, which enables efficient charge separation and charge transfer [17–19, 201, 202].

iii. **Band gap engineering.** Through introducing a secondary material of smaller band gap than the anatase TiO_2 [5, 203]. Visible spectral absorption is increased as a result of narrowing the resultant optical band gap of the heterostructure with TiO_2 nanotube layers [8, 12].

iv. **Co-catalysis effect**. By the decoration of catalyst metal nanoparticles, especially noble metals. A high work function metal particle at the surface of TiO_2 establishes a Schottky junction and restricts the charge carrier recombination. This enables the junction to capture more electrons in the conduction band and facilitate charge transfer process to the environment (aqueous, gas) [204].